RSC Advances

PAPER

View Article Online
View Journal | View Issue

Cite this: *RSC Adv.*, 2018, **8**, 18682

A modelling approach to assess the long-term stability of a novel microbial/electrochemical system for the treatment of acid mine drainage†

Emma Thompson Brewster, ‡ Guillermo Pozo,§ Damien J. Batstone, Stefano Freguia and Pablo Ledezma *

Microbial electrochemical processes have potential to remediate acid mine drainage (AMD) wastewaters which are highly acidic and rich in sulfate and heavy metals, without the need for extensive chemical dosing. In this manuscript, a novel hybrid microbial/electrochemical remediation process which uses a 3-reactor system – a precipitation vessel, an electrochemical reactor and a microbial electrochemical reactor with a sulfate-reducing biocathode – was modelled. To evaluate the long-term operability of this system, a dynamic model for the fluxes of 140 different ionic species was developed and calibrated using laboratory-scale experimental data. The model identified that when the reactors are operating in the desired state, the coulombic efficiency of sulfate removal from AMD is high (91%). Modelling also identified that a periodic electrolyte purge is required to prevent the build-up of Cl^- ions in the microbial electrochemical reactor. The model furthermore studied the fate of sulfate and carbon in the system. For sulfate, it was found that only 29% can be converted into elemental sulfur, with the rest complexating with metals in the precipitation vessel. Finally, the model shows that the flux of inorganic carbon under the current operational strategy is insufficient to maintain the autotrophic sulfate-reducing biomass. The modelling approach demonstrates that a change in system operational strategies plus close monitoring of overlooked ionic species (such as Cl^- and HCO_3^-) are key towards the scaling-up of this technology.

Received 13th April 2018
Accepted 14th May 2018

DOI: 10.1039/c8ra03153c

rsc.li/rsc-advances

Introduction

Production of acid and metalliferous mine drainage (AMD) is the result of atmosphere-exposed mining and processing of metal sulfide deposits for the extraction of numerous metals and minerals of commercial interest.[1] Safe management and disposal of AMD is a global environmental issue due to its highly-acidic nature, richness in heavy metals, strong chemical stability and lack of organics (that could facilitate its biological treatment).[2] Given these issues, the most common practice for AMD management worldwide is storage in dams plus evaporation, with significant environmental risks in the event of heavy rain/flooding, inadequate/insufficient storage dam capacity and soil/tectonic movements.[2] However, other options exist for both the prevention of AMD and its treatment. Other common treatment options include additional of alkaline chemicals to precipitate metals, ion exchange, adsorption and membrane technology.[3] Novel forms of AMD treatment offer opportunities for resource recovery. These include water recovery of sufficient quality for discharge or onsite reuse, as well as secondary minerals and/or metals of commercial interest.[4,5] Recently, our group has developed a hybrid autotrophic-microbial/electrochemical AMD treatment system that requires no chemical dosing and that is able to concomitantly produce a pH-neutral water effluent, recover elemental sulfur (S_0), produce a metal-sludge with superior settleability and that includes rare Earth elements and yttrium (REY) with numerous current and emerging industrial applications.[4]

Microbial electrochemical AMD remediation is nevertheless a relatively new proposed alternative to other conventional management/remediation methods[6] – such as neutralisation and precipitation by chemical dosing (of, for example, lime)[2] – meaning that questions remain open with regards to long-term system stability. For this purpose, and as complement to pilot-scale studies, the electrochemical model hereby presented evaluates the non-biological fluxes of 140 different ionic species and reveals potential issues with regards to the long-term operability and stability of the system we have proposed.[6]

Advanced Water Management Centre, The University of Queensland, St Lucia, QLD 4072, Australia. E-mail: p.ledezma@awmc.uq.edu.au; Fax: +61 7 3365 4726; Tel: +61 7 3346 3228

† Electronic supplementary information (ESI) available: ESI1: System schematic and modelling results; ESI 2: experimental data for model fitting; ESI 3: MATLAB codes. See DOI: 10.1039/c8ra03153c

‡ Present address: Centre for Mined Land Rehabilitation, Sustainable Minerals Institute, The University of Queensland, St Lucia, QLD 4072, Australia

§ Present address: Separation and Conversion Technologies, VITO-Flemish Institute for Technological Research, Boeretang 200, 2400, Mol, Belgium

Recently, modelling methods for electrochemical systems using wastewater (anaerobic digester liquor and source-separated urine[7,9]) as electrolyte have been developed. However, AMD contains lower concentrations of organics and nutrients, and higher concentrations of heavy metals and sulfate compared to these other streams, and has not been modelled in electrochemical systems before. There is, however, a strong background of equilibrium-based thermodynamic speciation models for geochemistry applications, which have been used to study AMD for decades.[10,11] MINTEQ,[12] PHREEQC[13] and other models are commonly employed for environmental risk assessments.[14] In particular, PHREEQC has been used to understand sulfate and pH remediation of AMD with coal fly ash,[15] and it has been combined with hydrologic models to study the ecological impacts of AMD releases.[16] The latest electrochemical models utilise speciation plus activity corrections to more accurately model the governing mechanisms of the processes, with speciation modelling methods detailed Flores-Alsina *et al.*[17] These methods have commonly been applied to domestic wastewater, but the solution principles are similar to MINTEQ and PHREEQC and should yield similarly valid outcomes to AMD related applications.[8]

In particular, while we have methodically studied the microbial and electrochemical transformation of sulfur, and flux of sulfur species in the laboratory,[6,18–20] the modelling approach hereby presented calculates the fluxes of up to 140 different ionic species present in the AMD. This is technically feasible but extremely complex to achieve experimentally. The results demonstrated provide valuable lessons for upcoming pilot-scale trials, including the accumulation of previously overlooked problematic ions in the system, such as carbonate species, Cl^- and NO_3^-. Microbial electrochemical technologies are a promising alternative for the treatment of mining wastewater with concomitant resource recovery, but their long-term stability and scalability is challenging. As a complement to pilot-scale trials, in this paper we present a mechanistic modelling approach to investigate these issues.

Materials and methods

Model configuration

The modelled system shown in Fig. 1 reflects the physical dimensions and operation of the hybrid microbial/electrochemical AMD treatment system developed by our group.[6] The treatment system (and its model accordingly) utilises three reactors (R1, R2 and R3) and three main recirculation loops that link these reactors hydraulically. The system operation can be summarised as follows (see Pozo *et al.*[6] for further details, and a detailed process configuration from Pozo *et al.*[6] is provided in Fig. S1† in the ESI†).

Raw AMD is fed into the precipitation tank (see R3 in Fig. 1), which is recirculated at a relatively high-flow-rate between the cathodic chamber of R2, a two-chamber electrochemical cell with an anion exchange membrane (AEM). The precipitation tank (R3) and the cathodic chamber of R2 are linked hydraulically and form what is referred to as the precipitation loop. In the experiments, a power source applied a fixed 1.7 V to R2, causing anions to migrate across the AEM. At this potential the expected electrode reactions in R2 at the anode is sulfide oxidation and at the cathode is water reduction. See further description of the electrode reactions below in the Electrode reactions section. Because most of the anions in the AMD feed are sulfate, migration mainly removes sulfate from the AMD and increases the pH in the precipitation tank (R3) from its acidic pH to a neutral controlled set point of 7.3. This neutral pH enables further removal of sulfate and heavy metals through precipitation of metal hydroxides and sulfides in R3. This is the main operational objective: treating the AMD for safe environmental discharge by removing sulfate and heavy metals and neutralising pH. Concomitantly, the system is able to recover elemental sulfur (S_0) through microbial and electrochemical reactions. The solution from the anode in R2 (which contains the migrated sulfate) is circulated to the biocathode of a microbial electrochemical cell (R1). The anodic chamber of R2 and the cathode chamber of R1 are called the central loop. The

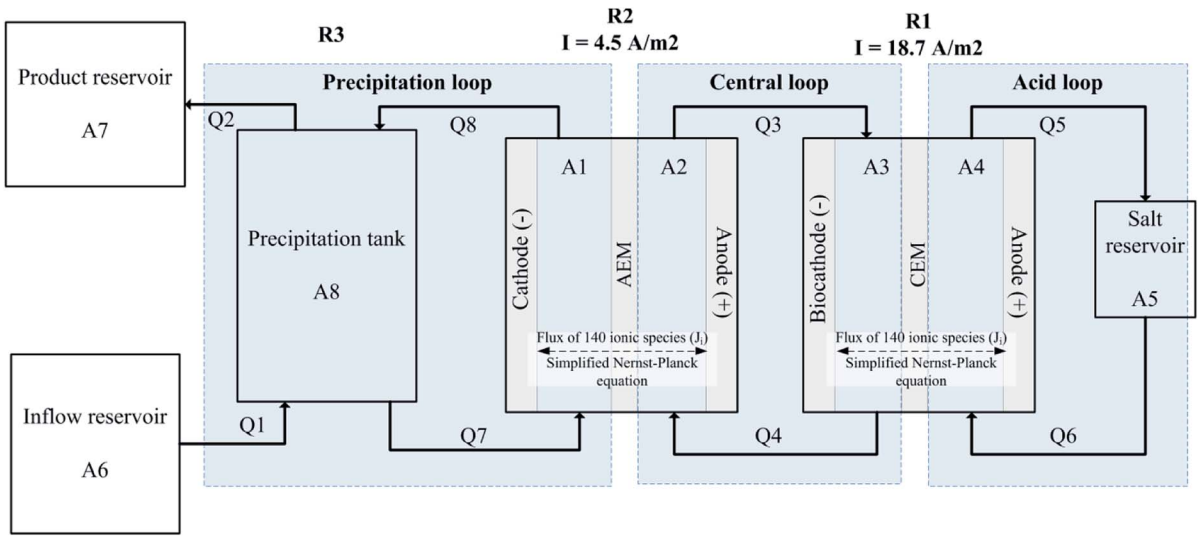

Fig. 1 Model configuration showing spatial areas (A1–A8), convective flows (Q1–Q8).

biocathodic reaction in R1 reduces sulfate to sulfide utilising the metabolism of autotrophic sulfate reducing bacteria (SRBs), and the anode of R2 electrochemically oxidises the sulfide produced by SRBs to elemental sulfur. The solution in the anodic chamber of R1 is looped onto an external reservoir (A5), which is called the acid loop. The pH of the acid loop is approximately pH 3, with migration in R1 mainly transporting protons across a cation exchange membrane (CEM) to help regulate the pH in the biocathode chamber A3.

The model (Fig. 1) has 8 spatial domains including: constant-volume catholytes and anolytes of R1 and R2 (A1 200 cm^3, A2 86 cm^3, A3 184.5 cm^3, A4 70.9 cm^3), a constant-volume precipitation vessel (A8 1800 cm^3), a constant-volume acidic recirculation reservoir (A5 29 cm^3), as well as varying volume feed and product reservoirs (A6, A7). In the laboratory experiments, A2 and A3 were packed with graphite granules with 43% porosity (El Carb 100, Graphite Sales Inc., USA), which is taken into account by modelled working volumes.[20,21] The modelled convective flow rates Q1 and Q2 were 0.03 L h^{-1} matching the average conditions of the laboratory experiments,[6] while the electrolytes in the precipitation loop (Q7, Q8), the central loop (Q3, Q4) and acid loop (Q5, Q6) are recirculated at a relatively fast speed (15 L h^{-1}). This fast speed is to model ideal mixing in the loops. The hydraulic retention time (HRT) for A8 is 60 h, while the HRT for A1, A2, A3, A4 and A5 are all less than 1 min. R1 had an effective membrane area of 121.85 cm^2 and R2 had an effective membrane area of 100 cm^2. Full MATLAB codes for this model (including instructions for use) can be found in the ESI 3.†

Initial conditions

There are three initial compositions used in the model, with the following compartments set equal to each other: feed initial composition, which is the same as the real AMD used in Pozo *et al.*[6] (A1, A6–A8), the initial concentrations in the central loop buffer solution prior to the start of the experiments (A2 and A3), and an initial salt solution (A4 and A5). The feed composition and initial concentrations in the model are provided in Table 1. The model simulates the later stages of the continuous experiments in Pozo *et al.*[6] However, the central loop buffer solution composition is only known for the conditions at the start of the experiments. Therefore the dynamic model requires a 15 d simulation start-up period for the model to reflect the conditions of the experimental data. The ionic strength of the feed solution is ~0.2 M. This ionic strength is not sufficiently high to be limiting in electro-concentration processes.[22,23]

Table 1 Initial concentrations used in the model

Component [mM]	Real AMD feed (A1, A6–A8)	Central loop buffer solution (A2, A3)	Salt solution (A4, A5)
Total sodium	63	130	0.62
Total potassium	1.0	22	0.18
Total ammonium	2.9	1.9	0
Total chloride	2.0	11	0
Total calcium	14	0.14	0
Total magnesium	24	0	0
Total carbonate	0.030	6.0	0
Total sulfate	110	16	0
Total phosphate	0.10	64	0.49
Total aluminium	18	0	0
Iron(II)	7.9	0	0
Iron(III)	2.3	0	0
Total nitrate	2.7	0	0

Precipitation reactions

In the experimental work, precipitation was observed both in the precipitation vessel (R3), as well as scaling on the cathode in A1 (R2). Undesired scaling/precipitation in A3 or A4 (R1) was not observed experimentally and is consequently not studied here. Instead of modelling scaling as several different terms, precipitation occurring on the cathode in A1 and in the precipitation reactor (R3) is included within a single sink term representing the overall precipitation. For practical purposes and considering the objective is to study the concentrations/fluxes in the aqueous phase, the model assumes all precipitation occurs in the precipitation tank (R3, A8). In A8, pH neutralisation removes nearly all the Al, Fe^{2+}, Fe^{3+}, Mg and Na, and some of the SO_4^{2-} from the liquid through continuous switch functions (eqn (1)). The residual threshold concentration parameter (K_i) was estimated for each component listed above through parameter estimation against experimental effluent concentrations (see Table 2).

$$r_i = \frac{C_{i,\mathrm{A8}} - K_i}{C_{i,\mathrm{A8}}} \quad (1)$$

where r_i is the rate of precipitation of component i, $C_{i,\mathrm{A8}}$ is the concentration of component i in the precipitation vessel and K_i represents the residual threshold concentration (mM). While this approach does not account for a mechanistic study of the electrode scaling or detailed insight into the precipitation products formed, it allows investigation of the sulfur species mass balances throughout the system. Time-resolved data of precipitates formed was not collected experimentally to allow

Table 2 Treated AMD values for major contaminants at the end of 15 d simulation compared with the average concentrations measured experimentally. Uncertainty is expressed as the 95% confidence interval

Component	Average measured experimental value [mM]	Modelled value at 15 d simulation [mM]
Effluent values		
Total sulfur	16.8 ± 1.6	16.7
Total sodium	21.3 ± 2.5	21.3
Total calcium	3.3 ± 0.4	3.3
Total magnesium	2.1 ± 0.2	2.0
Total iron	0.09 ± 0.03	0.02 (Fe^{2+} and Fe^{3+})
Total aluminium	0.001 ± 0.002	0.02
pH	7.2 ± 0.002	7.2
A2/A3 loop values		
Total sulfate	19.2 ± 3.2	19.0
Total sulfide	8.4 ± 3.3	8.4
Total chloride	40.3 ± 2.2	41.4
pH	~7.3	6.3

for a semi-mechanistic precipitation approach as in Kazadi Mbamba *et al.*,[24] nor have the authors found other work which describes the dynamic precipitation processes in an aqueous solution as complex as AMD. Further evaluation of electrode scaling is a suggested avenue of future study.

Ionic mass transport and speciation

Based on the ionic flux, pH and speciation methods developed in Thompson Brewster *et al.*,[7] the electrochemical (R2) and microbial electrochemical (R1) reactors were modelled using a Nernst–Planck equation, accounting for the speciation of different ionic species[17] and using a current proportioning method to describe membrane transport. Diffusion and migratory fluxes occurring across the anion exchange membrane (AEM) and cation exchange membrane (CEM) were represented by the Nernst–Planck equation and taking into account the components sodium, potassium, ammonium, chloride, acetate, calcium, magnesium, carbonate, sulfate, phosphate, aluminium, iron (2+), iron (3+), sulfide and nitrate, as well as acid–base pairing and ionic pairing. In this paper, components are referred to by the name of the component and species are referred to by the elemental symbol. The use of AMD compared to previously studied wastewaters[8,9] required the speciation code applied to electrochemical systems to be expanded to include aluminium, iron 2+ and iron 3+. Copper and nickel were not included as their concentrations in the AMD feed were 2 orders of magnitude lower than iron, aluminium, calcium and magnesium, and that they are not included in the speciation code from Flores-Alsina *et al.*[17] Copper and nickel would likely precipitate in the precipitation vessel (R3) to even lower aqueous concentrations, and their inclusion in the model would not influence the key findings.

The experimental current densities for both reactors were stable with the current density in R1 (I_1) being 18.7 ± 0.001 A m^{-2} and R2 (I_2) being 4.5 ± 0.005 A m^{-2}, with uncertainty expressed here as the 95% confidence interval. Due to the high stability, the average values for current density were used in the model. No diffusion boundary layers (DBLs) were taken into account in the modelling as at the large chamber widths utilised, these were unlikely to be a limiting mechanism.[7]

Electrode reactions

Implicit water splitting reactions were included at the R2 cathode and R1 anode based on the ionic fluxes of major ionic species (*i.e.* species not H^+ or OH^-), to evaluate the pH effect from these electrode reactions (eqn (2) and (3), respectively). Explicit electrochemical oxidation of HS^- to S_0 was included for the R2 anode (eqn (4)), as well as the implicit cathodic water splitting and explicit biofilm reaction of sulfate to HS^- at the R1 biocathode (eqn (5) and (6), respectively).

$$2H_2O + 2e^- \rightarrow H_{2(g)} + 2OH^- \quad (2)$$

$$4H_2O \rightarrow 8H^+ + 8e^- + 2O_2 \quad (3)$$

$$HS^- \rightarrow S_{0(s)} + H^+ + 2e^- \quad (4)$$

$$8H^+ + 8e^- \rightarrow 4H_2 \quad (5)$$

$$4H_2 + SO_4^{2-} + H^+ \rightarrow HS^- + 4H_2O \quad (6)$$

The experiments and model were run such that the current density of R1 (relating to the biocathodic sulphur reduction reactions in eqn (5) and (6)) is 4.1 times that of R2 (relating to the oxidation to form elemental sulphur in eqn (4)). This accounts for the 8 : 2 ratio of electrons required for eqn (5) and (6), and eqn (4), respectively. When modelling the system, it became evident that the reagents of the key explicit reactions (eqn (4) and (6)) are limiting, and the reactions do not occur at 100% coulombic efficiency (CE). Practically, this means there are additional electrode reactions occurring. In particular, at the R2 anode at least one of the following reactions necessarily occurs: (i) elemental sulfur oxidation to sulfate, (ii) water oxidation to O_2, and/or (iii) H_2 oxidation to water. The effects of these additional reactions are modelled as implicit water splitting (eqn (2) and (3)). A continuous switch function was used to regulate the source or sink rates for the explicit electrode reactions based on the reactive species and a constant, K_1 or K_2, representing the residual threshold concentration of the reactant required for the reaction to proceed. Eqn (7)–(10) show how the rates of explicit reactions were calculated for the R1 biocathode (eqn (7) and (8)) and the R2 anode (eqn (9) and (10)).

$$r_{SO_4,A3} = -\left(\frac{C_{SO_4,A3} - K_1}{C_{SO_4,A3}}\right) \frac{I_1 A_{m1}}{8F} \quad (7)$$

$$r_{HS,A3} = -r_{SO_4,A3} \quad (8)$$

$$r_{HS,A2} = -\left(\frac{C_{HS,A2} - K_2}{C_{HS,A2}}\right) \frac{I_2 A_{m2}}{2F} \quad (9)$$

$$r_{S_0,A2} = -r_{HS,A2} \quad (10)$$

where A_{m1} and A_{m2} (m^2) are the effective membrane areas in R1 and R2, respectively, and F is Faraday's constant (96 485 C mol^{-1}).

H_2O_2 production at the cathode in the presence of oxygen is a topic discussed in the electrochemical remediation literature.[25] The cathode water splitting reaction in eqn (2) may complete with the reaction in eqn (11), producing H_2O_2.

$$2H_2O + O_2 + 2e^- \rightarrow H_2O_2 + 2OH^- \quad (11)$$

These two reactions (eqn (2) and (11)) remove the same charge, producing the same net effect on pH and hence reaction (11) can be implicitly included as for reaction (2) (since H_2 and O_2 are not considered as states). This study focuses on OH^- formation. Therefore, the presence of oxygen at the cathode is assumed to not affect the estimation of OH^- formation. If H_2O_2 and HO_2^- are not involved with speciation or ion pairing, the pH model output is unaffected. It is possible, but extremely unlikely, to have H_2O_2 production in the cathode of the electrochemical reactor R2 (A1), since R2 is operated at a fixed 1.7 V, resulting in a low cathode potential that would produce H_2 and convert H_2O_2 to H_2O immediately. In addition, dissolved oxygen would need to be present in the AMD feed solution to produce H_2O_2.

Results and discussion

Model output and validation

Fig. 2 displays some key model outputs for a 30 d simulation. The model was run using the fitted parameters of $K_1 = 3.7$ mol m^{-3} and $K_2 = 0.55$ mol m^{-3} for the explicit electrode reactions by comparing the model results with the experimental data shown in Table 2. For each of the precipitation sinks, the following parameters were fitted: $K_{Al} = 0.005$, $K_{Ca} = 1.9$, $K_{Fe_2} = 0.01$, $K_{Fe_3} = 0.01$, $K_{Mg} = 0.17$, $K_{Na} = 17.7$, $K_{PO_4} = 0.01$ and $K_{SO_4} = 12.45$.

Fig. 2 demonstrates 30 d of simulation. At which point the system becomes unstable. The key outcome of the paper is demonstrating that long-term system operation is unstable. Followed by discussion on why it is so, and suggestions for long-term operability. As can be observed in Fig. 2, the model did not reach steady-state within the 30 d period. Running the model for a longer duration would not provide additional information as after 17 d the model no-longer reflected appropriate operation of the system, as discussed further below. The desired operation state of the system occurs between 10–16 days of simulation time. For this section of the discussion, the model operation at 15 d simulation time will be discussed. Afterwards, operational strategies to maintain steady state will be described.

The model was calibrated against a period of relatively steady data collected in the laboratory, when the experimental system successfully and continuously neutralised the AMD to pH = 7.3 and removed sulfate at a rate of 0.946 ± 18 kg SO_4-S m^{-3} d^{-1} (referred to as Period IV of the experiments in Pozo *et al.*[6]). Due to limited experimental data for the initial conditions and no long-term steady-state experimental data, the goal of the model validation is to demonstrate there is representative similarity between the simulation and the observations. The model therefore can be used to better understand the fluxes of major ions and the relationships between ionic composition and pH in the microbial/electrochemical system.

The calibration data was averaged from the experimental data shown in the ESI-2† spreadsheet from Pozo *et al.*[6] While the measured concentrations were relatively constant, measurements were not taken of all ionic species in solution (for example, chloride and nitrate were not measured). In addition, the measured data did not demonstrate long-term steady-state conditions for all species, even if the stability of the electrical performance appeared to indicate so (see above, current densities with 95% confidence intervals ≤ ± 0.005 A m^{-2}). The laboratory experimental data set includes effluent concentrations of iron, magnesium, manganese, sodium, nickel, lead, sulfur, zinc and pH from R3 (A8) and the sulfate, sulfite and chloride concentrations in the central loop. To demonstrate the representative similarity between the model and experiments, model conditions at the end of 15 d simulation time were compared with the average values in the experimental data, as shown in Table 2. See Fig. S2–S5 in the ESI† for raw model output. At 15 d simulation time, the model demonstrates conditions within the 95% confidence intervals of most of the experimental observations. The exception is the pH of the A2/A3 central loop in which the pH is low (6.4, compared to the desired value of 7.3). However, it is worth noting that this pH discrepancy reflects a difference of approximately 1 mM of concentration imbalance from the major ions, which is within reasonable variance of the experimental observations shown below.

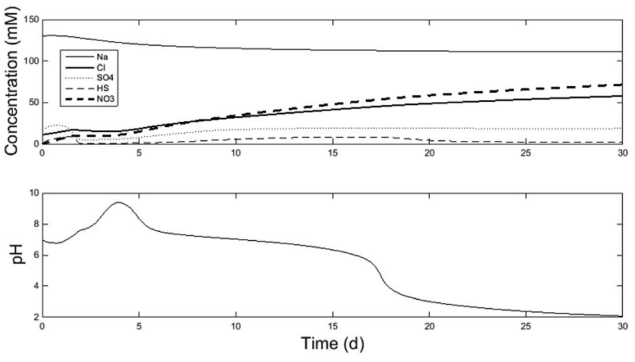

Fig. 2 30 d model simulation demonstrating of anion accumulation in the central loop (A2/A3) and the resulting decrease in pH. See further details of species concentration and pH evolution per reactor chamber in the ESI.†

Coulombic efficiencies (CE) of the explicit electrode reactions

The following results describe the conditions at 15 d simulation time, which reflects the desired operational conditions. The CE of the sulfate removal equation (eqn (6)) in A3 is 81% and elemental sulfur production (eqn (4)) in A2 is 93%. The model reflects the experimental observations with targeted explicit reactions having a high CE (>80%) as estimated experimentally (85 ± 2%).[6] While the modelled equations used for these reactions are simplified compared the complexity of the real life conditions, particularly for the biocathodic reaction in R1, the modelled CEs (based on a mass balance independent of the reaction pathway complexity) illustrate similarity to the data.

Ion transport across the AEM in reactor 2

Efficiency of SO_4^{2-} transport. To maintain high CE levels for SO_4^{2-} migration, it is essential that the pH of the precipitation vessel (R3) and R2 are close to the set point of 7.3. If the pH in R3 increases above this set point, hydroxide ions may begin to migrate and pass charge across the AEM *in lieu* of SO_4^{2-}, which would decrease the efficiency of the process.[9] As shown in Fig. 3, 91% of the total current in R2 is used to migrate SO_4^{2-} across the AEM from the AMD solution into the anodic chamber of R2 (*i.e.* from A1 to A2). Other species transported into A2 are Cl^-, NO_3^- and $NaSO_4^-$, while some species were found to transport in the opposite direction (A2 to A1), including H^+, Na^+ and $H_2S_{(aq)}$. The rates of migration of each species are proportional to the activity, charge and Fickian diffusion coefficient as described in Thompson Brewster *et al.*[7] Sulfate provides 96% of the anions (in [mol]) in the feed, resulting in a high coulombic efficiency for its migration, but there will always be co-transport by other anions and undesired back-diffusion of species (for example, Na^+ and H^+) where the concentration gradient across

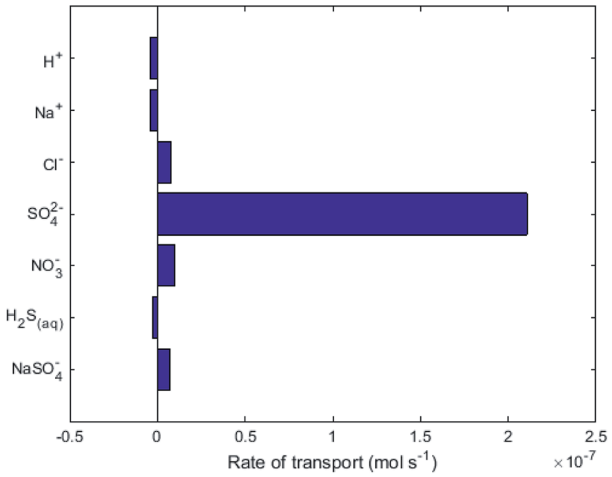

Fig. 3 Rate of transport of the highest flux ions across the AEM in R2. Positive values indicate the intended direction (*i.e.* from cathode to anode).

the membrane results in diffusion in the direction opposite to migration.

Carbonate transport. A critical consideration of the long-term operability of this system is whether the small amount of inorganic carbon in the acid-mine drainage solution (0.03 mM) will migrate into the A2/A3 central loop to supply sufficient carbon (as a nutrient) for the autotrophic microorganisms on the biocathode.[26,27]

While no biological carbon consumption was modelled here, looking at the fluxes of the carbon containing species can give some insight. Fig. 4 shows the rates of ionic transport of carbon-containing species at 15 d of simulation time; note that the *x*-axis scale in Fig. 4 is 3 orders of magnitude smaller than in Fig. 3. The results indicate that at 15 d operation time, $H_2CO_{3(aq)}$ is transporting carbon out of the central loop (*i.e.* away from the biocathode) due to diffusion at a rate higher than HCO_3^- is migrating towards the biocathode. This is largely due to the relatively-higher concentrations of $H_2CO_{3(aq)}$ in the central loop compared to the precipitation loop.

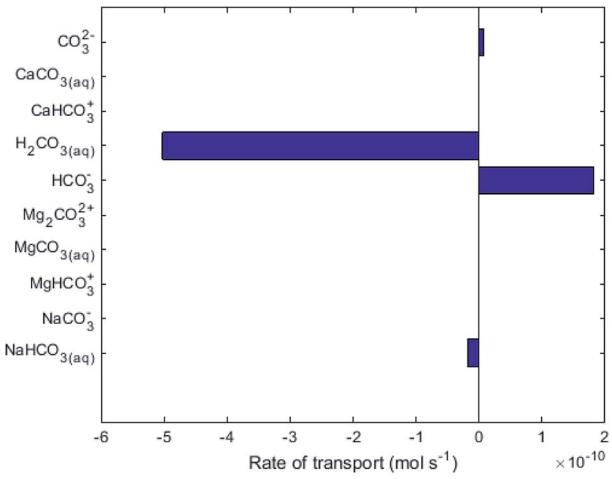

Fig. 4 Rate of transport of the species containing carbon across the AEM in R2. Positive values indicate the intended direction (from cathode to anode).

Fig. 4 shows that some HCO_3^- (2×10^{-10} mol s^{-1}) does migrate from the AMD into the central loop. While the conditions set in the model do not support that there can be a net flux of carbon into the central loop (Q3, Q4, A2 and A3 in Fig. 1). To provide the biomass with this essential nutrient, different operational conditions could promote a net flux of carbon-containing species in the desired direction based on the Nernst–Planck equation discussed in Thompson Brewster *et al.*[7] If the central loop carbonate concentrations were lower than seen here, because either the buffer solution contained less carbonate initially, or the biological activity consumed a sufficient amount of carbonate, this would reduce the back-diffusive driving force, allowing migration of HCO_3^- and CO_3^{2-} towards the biocathode to be the dominant form of carbon flux (to sustain the biomass). The model shows that attention is needed to ensure that C is not limiting for the maintenance of the autotrophic SRB biomass when up-scaling the proposed technology. This should be done in consideration of the known metabolic flexibility of SRBs,[28] either by controlling the carbonate transport as discussed above or (less-ideally) by chemical addition of, for example, bicarbonate salts.

Long-term operation. The 30 d simulation shown in Fig. 2 clearly illustrates that the AMD treatment system under its current configuration cannot run stably beyond 17 d. The modelling reveals that while the levels of SO_4^{2-} can be controlled due to the explicit electrode reactions, no such mechanism exists in the current design to actively remove Cl^- and NO_3^- ions in the central loop leading to their unwanted accumulation over time. Nitrate reduction by microbial biocathodes is a well-established metabolic capability[29,30] that could potentially be enriched in a mixed-culture biocathode that also contains SRBs. However, there is currently no viable biological/electrochemical mechanism to remove Cl^- that would not significantly affect the process in other ways (for example, electrochemical chlorine evolution could be possible at higher applied voltages in R2). Considering that for chlorine evolution the $E_0' = +1.36$ V and the inherent overpotential of the carbon electrodes hereby utilised,[31] this would require a significantly higher applied voltage than the 1.7 V used for R2 for chlorine evolution to occur. If chlorine evolution did happen it would be deleterious for the linked biocathode of R1, but it is unlikely to occur under the existing operational conditions.

Fig. 3 shows that the net flux of anions (primarily Cl^- and NO_3^-) will eventually cause a decrease of pH in the central loop to below biological limits (<4), due to unintended anode reactions at A2 (*i.e.* reactions which are not eqn (4)). These unintended reactions were modelled here as oxygen evolution, but in reality they could also be reformation of sulfate from elemental sulfur. Accumulation of anions, Cl^- and NO_3^- in the central loop will result in a drop in pH, due to the charge balance relating to speciation modelling.[17] These results indicate that a constant or periodical purge of the electrolyte from the central loop would be necessary as part of the operational strategy to remove the build-up of Cl^- beyond physiological pH limitations. A constant electro-osmotic flux of water will occur into the

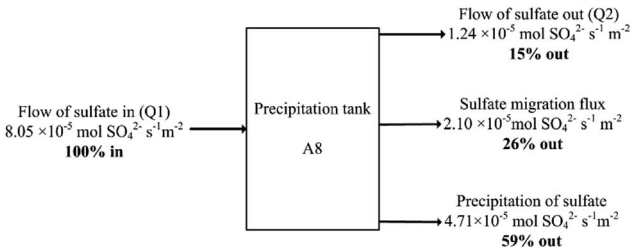

Fig. 5 Sulfate balance over the precipitation reactor normalised per membrane areas of the R2 anion exchange membrane (0.01 m^2) at 15 d simulation time.

central loop due to the migration of hydrated ions.[32,33] If this small flux of water was matched in volume by a purge this would result in Cl^- concentrations reaching a steady value, therefore preventing the pH crash. The electroosmotic flux should be determined experimentally in order to implement and validate a water flux model as in Pronk *et al.*[32] For a pilot-scale system, a level control loop could be installed in an external recirculation reservoir for the central loop, with the reservoir level maintained constant *via* a feedback control loop.

Another application consideration is variation in influent composition. Feed composition would be different at different treatment sites, but also at the same site over time due to geochemical weathering and rainfall events. Chemical pH neutralisation is a commonly used treatment across many AMD sites, and electrochemical pH neutralisation should work similarly. However, ensuring the biocathode has stable conditions would be of importance.

Fate of sulfate in the system. Fig. 3 shows that under pseudo-steady-state conditions (*i.e.* day 15 in Fig. 2), the fitted rate of SO_4^{2-} migration across the AEM into the central loop is 2.1 × 10^{-5} mol SO_4^{2-} s^{-1} m^{-2}. Based on this, a simple steady state mass balance of the A8 space (R3 + R2 domains) was calculated and illustrated in Fig. 5. The results indicate that approximately 59% of the influent SO_4^{2-} precipitates in R3, rather than migrating for biological reduction at R1 and subsequent precipitation as S_0 *via* electrochemical oxidation in R2. It is assumed that all SO_4^{2-} that migrates out of A8 eventually is transformed to S_0, as there is no evidence or modelled mechanism otherwise.

The case for S_0 recovery would not become more favourable even at 100% CE efficiency for SO_4^{2-} transport, as this would only remove 2.33 × 10^{-5} mol SO_4^{2-} s^{-1} m^{-2} through the AEM (see Fig. 1), which would mean 26% of the total SO_4^{2-} entering the system. Precipitation of sulfate in the R3 does not appear to be detrimental to process operation, and it lowers the load on the microbial and electrochemical cells R1/R2, which would mean reduced reactor sizes and thus lower AMD remediation costs when compared to a 100% sulfate-to-sulfur conversion.

Conclusions

The model hereby presented studied the fluxes of 140 ionic species in a novel 3-reactor microbial/electrochemical reactor configuration designed to treat AMD without chemical additions. The results confirm that the proposed treatment system can achieve relatively high (≥80%) coulombic efficiencies for its explicit electrochemical reactions. However, some key limitations and valuable lessons towards pilot-scale trials were also discovered. Firstly, in order to achieve steady-state operation with stable pH, a regular liquid purge of the central loop is required to prevent the pH from dropping due to Cl^- ion accumulation. Secondly, a mass balance analysis showed that the majority (59%) of the removed sulfate would precipitate in R3 (the precipitation reactor) and only 26% would be converted to S_0 in R2. This decreases system loading and therefore sizing and costs, but means S_0 recovery cannot not be a significant focus of the process. The recovery should therefore probably focus on valuable REY elements rather than S_0. A final limitation is that the mass flux of carbon from the AMD to the central loop as HCO_3^- is insufficient to maintain the autotrophic biofilms over time. A small carbon source from the AMD (approximately 2 × 10^{-8} mol C s^{-1} m^{-2}) was observed. However, the operational conditions have to be changed in order to reduce undesirable H_2CO_3 diffusion to process areas away from the biomass. The total C migration should be monitored through longer term studies to ensure carbon supply for the microbes can be met. Long-term operation considerations relating from membrane and electrode scaling were not covered in this paper, but are an important avenue of future work and will be included in the pilot-scale study.

Conflicts of interest

The authors declare no conflict of interest.

Acknowledgements

The authors thank the Australian Research Council for funding support through Discovery Project DP120104415. G. Pozo acknowledges a Chilean Scholarship (Becas Chile) from the National Commission for Science Research and Technology (CONICYT) of Chile. P. Ledezma acknowledges an ECR Development Fellowship from The University of Queensland.

References

1 J. Phillips, *Applied Geography*, 2016, **74**, 95–108.
2 D. B. Johnson and K. B. Hallberg, *Sci. Total Environ.*, 2005, **338**, 3–14.
3 K. K. Kefeni, T. A. M. Msagati and B. B. Mamba, *J. Cleaner Prod.*, 2017, **151**, 475–493.
4 O. Modin and F. Aulenta, *Environ. Sci.: Water Res. Technol.*, 2017, **3**, 391–402.
5 Y. Feng, L. Yang, J. Liu and B. E. Logan, *Environ. Sci.: Water Res. Technol.*, 2016, **2**, 800–831.
6 G. Pozo, S. Pongy, J. Keller, P. Ledezma and S. Freguia, *Water Res.*, 2017, **126**, 411–420.
7 E. Thompson Brewster, C. M. Mehta, J. Radjenovic and D. J. Batstone, *Water Res.*, 2016, **94**, 176–186.
8 E. Thompson Brewster, J. Jermakka, S. Freguia and D. J. Batstone, *Water Res.*, 2017, **124**, 210–218.

9 E. Thompson Brewster, A. J. Ward, C. M. Mehta, J. Radjenovic and D. J. Batstone, *Water Res.*, 2017, **110**, 202–210.
10 E. H. Perkins, H. W. Nesbitt, W. D. Gunter, L. C. St-Arnaud and J. R. Mycroft, *Critical Review of Geochemical Processes and Geochemical Models Adaptable for Prediction of Acidic Drainage from Waste Rock, Energy, Mines and Resources Canada*, Centre for Mineral and Energy Technology, 1995.
11 B. S. Caruso, T. J. Cox, R. L. Runkel, M. L. Velleux, K. E. Bencala, D. K. Nordstrom, P. Y. Julien, B. A. Butler, C. N. Alpers, A. Marion and K. S. Smith, *Hydrol. Processes*, 2008, **22**, 4011–4021.
12 J. D. Allison, D. S. Brown and K. J. Novo-Gradac, *MINTEQA2/PRODEFA2, a geochemical assessment model for environmental systems: version 3.0 user's manual*, Environmental Research Laboratory, Office of Research and Development, U.S. Environmental Protection Agency, Athens, GA. 1991.
13 D. L. Parkhurst and C. A. J. Appelo, *User's guide to PHREEQC (Version 2): a computer program for speciation, batch-reaction, one-dimensional transport, and inverse geochemical calculations*, Report 99–4259, 1999.
14 G. D. Betrie, R. Sadiq, C. Nichol, K. A. Morin and S. Tesfamariam, *J. Hazard. Mater.*, 2016, **301**, 187–196.
15 G. Madzivire, W. M. Gitari, V. R. K. Vadapalli, T. V. Ojumu and L. F. Petrik, *Miner. Eng.*, 2011, **24**, 1467–1477.
16 N. Papassiopi, C. Zaharia, A. Xenidis, K. Adam, A. Liakopoulos and I. Romaidis, *Miner. Eng.*, 2014, **64**, 78–91.
17 X. Flores-Alsina, C. Kazadi Mbamba, K. Solon, D. Vrecko, S. Tait, D. J. Batstone, U. Jeppsson and K. V. Gernaey, *Water Res.*, 2015, **85**, 255–265.
18 G. Pozo, L. Jourdin, Y. Lu, P. Ledezma, J. Keller and S. Freguia, *RSC Adv.*, 2015, **5**, 89368–89374.
19 G. Pozo, L. Jourdin, Y. Lu, J. Keller, P. Ledezma and S. Freguia, *Electrochim. Acta*, 2016, **213**, 66–74.
20 G. Pozo, Y. Lu, S. Pongy, J. Keller, P. Ledezma and S. Freguia, *Bioelectrochemistry*, 2017, **118**, 62–69.
21 S. Freguia, K. Rabaey, Z. Yuan and J. Keller, *Electrochim. Acta*, 2007, **53**, 598–603.
22 A. J. Ward, K. Arola, E. Thompson Brewster, C. M. Mehta and D. J. Batstone, *Water Res.*, 2018, **135**, 57–65.
23 J. Jermakka, E. Thompson Brewster, P. Ledezma and S. Freguia, *Sep. Purif. Technol.*, 2018, **203**, 48–55.
24 C. Kazadi Mbamba, S. Tait, X. Flores-Alsina and D. J. Batstone, *Water Res.*, 2015, **85**, 359–370.
25 H. H. Yang and R. L. McCreery, *J. Electrochem. Soc.*, 2000, **147**, 3420–3428.
26 K. Jansen, R. K. Thauer, F. Widdel and G. Fuchs, *Arch. Microbiol.*, 1984, **138**, 257–262.
27 K. Brysch, C. Schneider, G. Fuchs and F. Widdel, *Arch. Microbiol.*, 1987, **148**, 264–274.
28 C. M. Plugge, W. Zhang, J. C. M. Scholten and A. J. M. Stams, *Frontiers in Microbiology*, 2011, **2**, 81.
29 B. Virdis, K. Rabaey, R. A. Rozendal, Z. Yuan and J. Keller, *Water Res.*, 2010, **44**, 2970–2980.
30 B. Virdis, K. Rabaey, Z. Yuan and J. Keller, *Water Res.*, 2008, **42**, 3013–3024.
31 K. S. Exner, J. Anton, T. Jacob and H. Over, *Angew. Chem., Int. Ed.*, 2016, **55**, 7501–7504.
32 W. Pronk, M. Biebow and M. Boller, *Environ. Sci. Technol.*, 2006, **40**, 2414–2420.
33 P. Ledezma, J. Jermakka, J. Keller and S. Freguia, *Environ. Sci. Technol. Lett.*, 2017, **4**, 119–124.